Finite temperature behavior of impurity doped Lithium cluster, Li_6Sn

Kavita Joshi[a] and D. G. Kanhere
Department of Physics, University of Pune, Ganeshkhind, Pune 411 007, India

(Received 22 May 2003; accepted 26 September 2003)

We have carried out extensive isokinetic *ab initio* molecular-dynamic simulations to investigate the finite temperature properties of the impurity doped cluster Li_6Sn and the host cluster Li_7. The data obtained from about 20 temperatures and total simulation time of at least 3 ns is used to extract thermodynamical quantities like canonical specific heat. We observe that, first, Li_6Sn becomes liquidlike around 250 K, at much lower temperature than that for Li_7 ($\approx$425 K). Second, a weak shoulder around 50 K in the specific heat curve of Li_6Sn is observed due to the weakening of Li–Li bonds. The peak in the specific heat of Li_7 is very broad and the specific heat curve does not show any premelting features. © *2003 American Institute of Physics.* [DOI: 10.1063/1.1626538]

I. INTRODUCTION

Small clusters are known to behave differently than their bulk counterparts, mainly because of their finite size. The finite size effects are reflected in most of their properties, like equilibrium geometries, energetics, optical properties, ionization potential, polarizabilities, etc.[1–5] For example, equilibrium geometries of small as well as medium size clusters are considerably different than the bulk structures. Stability of a class of clusters depends on the filling up of geometric or electronic shell. The well-known example of such a stability is that of alkali metal clusters displaying magic numbers. Further, the properties of homogeneous clusters may be altered, some times quite significantly by adding an impurity. In the last few years some work has been reported on the impurity doped clusters.[6,7] These studies have brought out a number of interesting aspects like trapping of an impurity, modifications in the equilibrium structures, changes in the bonding characteristics and enhancement or otherwise in the stability. A few studies have also been reported on the optical properties. Many of these properties have been shown to get influenced by the relative difference in the valence, ionic radii, and electro-negativity.

A majority of the investigations on heterogeneous and homogeneous clusters pertain to the ground state properties. During the last few years a number of experimental[8,9] and theoretical[10–12] studies on finite temperature behavior of clusters have been reported. Finite temperature behavior of homogeneous clusters turns out to be very intriguing and has brought out many interesting features in contrast to the bulk behavior.[13] For instance, clusters exhibit a broad peak in the specific heat which is sometimes accompanied by a premelting feature like a shoulder indicating possible isomarization. Recent experiments[9] and simulations[11,12] on tin clusters have shown that these clusters become liquidlike at higher temperatures than the bulk melting temperature (Tm_{bulk}) contrary to the belief that solidlike to liquidlike transition in the finite size systems occurs at a temperature lower than Tm_{bulk} because of the surface effects. A number of experiments on Na clusters by Haberland and co-workers[8] have demonstrated that there is no systematic size dependence observed in the melting temperature of clusters between sizes 50 and 200. More interestingly, the peaks in the melting temperature as function of size do not occur at the geometric or electronic shell closing.

In the present work, we investigate the finite temperature behavior of Li_6Sn and Li_7. Since the impurity is known to change the geometry as well as bonding substantially in the host cluster it is also expected to change the finite temperature properties of the host cluster. The motivation for carrying out detailed thermodynamic investigations of these clusters comes from our previous study of Sn doped Li clusters.[14] This study has shown that, doping of lithium cluster with a tetravalent impurity such as Sn, induces a charge transfer from Li to Sn and as a result the nature of bonding changes from metallic like to dominantly ionic like. Preliminary investigation of the finite temperature behavior of Li_6Sn indicated that this charge transfer induces dramatic effects at low temperatures. The interest in these systems also stems from the anomalous behavior seen in the bulk properties (e.g., electrical resistivity, density, stability function) of Li-Group IV alloys as a function of composition.[15] These alloys show peak in the resistivity around 20% Sn composition and this has been interpreted as atomic clustering around Sn at this composition whereas other alkali metal-Group IV alloys show peak in the resistivity around 50% composition of Group IV elements. It has also been observed that Li–Si alloys[16] show 15% volume contraction in the liquid state for Si concentration between 15% and 50% whereas in Na–Sn alloys[17] melting takes place via *rotor* phase in which alkali atoms are suppose to diffuse freely while the group IV polyanions perform only rotational or vibrational movement.

As we shall demonstrate in this paper, addition of an impurity has significantly lowered the ''melting'' temperature of the cluster. In addition, the impurity also induces a constrained motion of alkali atoms around Sn at low temperatures. Further, in the liquidlike state the value of root mean square bond length fluctuations (δ_{rms}) of impurity doped cluster turns out to be considerably lower than that of Li_7 indicating that volume expansion upon melting is much

[a]Electronic mail: kavitaj@unipune.ernet.in

less in this cluster. Although it is difficult to establish a direct correlation between the properties of the bulk alloys and a small cluster like Li_6Sn, we believe that the physics of impurity induced effects in both the systems essentially has the same origin arising out of the charge transfer which results into the strong ionic bond.

It is now well established that for reliable ion dynamics one must reproduce the bonding properly. Description of ion dynamics critically depends on the correct microscopic description of instantaneous state of electrons as system evolves in time. This is especially true when the nature of bonding may change during evolution of the trajectories at different temperatures. Therefore, for obtaining reliable ion dynamics we have chosen to use density-functional theory (DFT). Small size of the system has permitted us to perform *ab initio* calculations for substantially larger simulation time as compared to the previously published *ab initio* results.[10–12]

The paper is organized as follows. In Sec. II we describe briefly our computational and statistical approaches. Results for the equilibrium geometries, nature of bonding and finite temperature properties of Li_7 and Li_6Sn are given in Sec. III, and the conclusions are given in Sec. IV.

II. COMPUTATIONAL DETAILS

All the calculations have been performed using the Kohn–Sham formulation of density-functional molecular dynamics (MD),[18] using the nonlocal norm-conserving pseudopotentials of Bachelet *et al.*[19] in Kleinman–Bylander form[20] with the Ceperley–Alder[21] exchange-correlation functional. A cubic supercell of length 30 a.u. is used with energy cutoff of 15 Ry. for Li_6Sn and 12 Ry. for Li_7, which is found to provide sufficient convergence in total electronic energy ($E_{\rm tot}$). To have a sufficiently precise evaluation of the Hellmann–Feynman forces on the ions, we ensure that the residual norm of each KS orbital, defined as $|H_{\rm KS}\psi_i - \epsilon_i\psi_i|^2$ (ϵ_i being the eigenvalue corresponding to eigenstate ψ_i of the KS Hamiltonian $H_{\rm KS}$), was maintained at 10^{-12} a.u. After every ionic movement the total electronic energy is converged up to 10^{-5} a.u. for low temperatures ($T \leqslant 200$ K) and the convergence is 10^{-4} a.u. for higher temperatures. Such a high convergence is not warranted in the simulated annealing runs but it is very crucial for probing finite temperature behavior of impurity doped clusters. The ground state and other equilibrium structures have been found by carrying out several steepest-descent runs starting from structures chosen periodically from a high-temperature simulation.

The ionic phase space is sampled by isokinetic MD,[22] in which the kinetic energy is held constant using velocity scaling. For Li_7 we split the temperature range $100\,{\rm K} \leqslant T \leqslant 1000$ K into about 20 different temperatures, performing up to 90 ps of simulation for lower temperatures (i.e., $T \leqslant 200$) and 150–200 ps for higher temperatures. For Li_6Sn we split the temperature range $10\,{\rm K} \leqslant T \leqslant 900$ K into about 23 different temperatures, performing up to 200 ps of simulation for lower temperatures (i.e., $T \leqslant 200$) and 150 ps for higher temperatures. This results into total simulation time about 3 ns for Li_7 and 5 ns for Li_6Sn.

The data obtained from these extensive simulations is used to extract different thermo-dynamic quantities such as entropy, specific heat, etc. The ionic specific heat is calculated from the fluctuations in the internal energy of the system and is given by

$$C(T) = \frac{3Nk_B}{2} + \frac{1}{k_B T^2}(\langle V^2\rangle_t - \langle V\rangle_t^2), \tag{1}$$

where V is total electronic energy and $\langle\cdots\rangle_t$ denotes time averaged over the entire trajectory. A smooth specific heat can be obtained by using multiple histogram (MH) technique.[23] With multihistogram fit, which is basically a least-square fit we extract density of states $[\Omega(E)]$ or entropy $[S(E) = k_B \ln \Omega(E)]$. From entropy we can compute various thermodynamic quantities like canonical specific heat, $C(T) = \partial U(T)/\partial T$, where $U(T) = \int Ep(E,T)dE$ is the average total energy, and where the probability of observing an energy E at a temperature T is given by the Gibbs distribution $p(E,T) = \Omega(E)\exp(-E/k_BT)/Z(T)$, with $Z(T)$ the normalizing canonical partition function.

Along with these thermodynamic quantities we also analyze the data using phenomenological indicators such as $\delta_{\rm rms}$ and power spectra $C(\omega)$.

The $\delta_{\rm rms}$ is defined as

$$\delta_{\rm rms} = \frac{2}{N(N-1)}\sum_{I>J}\frac{(\langle R_{IJ}^2\rangle_t - \langle R_{IJ}\rangle_t^2)^{1/2}}{\langle R_{IJ}\rangle_t}, \tag{2}$$

where N is the number of ions in the system, R_{IJ} is the distance between ions I and J, and $\langle\cdots\rangle_t$ denotes a time average over the entire trajectory.

The power spectrum, which is a Fourier transform of velocity auto correlation is defined as

$$C(\omega) = 2\int_0^\infty C(t)\cos(\omega t)dt, \tag{3}$$

with velocity autocorrelation $C(t)$ is defined as

$$C(t) = \frac{\langle (v(t_0+t) - \langle v\rangle)\cdot(v(t_0) - \langle v\rangle)\rangle}{\langle (v(t_0) - \langle v\rangle)^2\rangle}. \tag{4}$$

We would like to make few pertinent comments on some technical issues which are specific to *ab initio* simulations. Since such DFT simulations are quite expensive, a judicious choice of simulation time step (Δt), criteria for the convergence in the total electronic energy during Born–Oppenheimer MD ($\Delta E_{\rm SCF}$) and total simulation time has to be made. Some of these issues may not be very crucial for geometry optimization, since there the details of ion dynamics are secondary. However, for reliable extraction of thermodynamic data, the ion dynamics should be faithfully simulated using the accurate forces. Since the calculation of forces involves the total electronic energy ($E_{\rm tot}$), the choice of $\Delta E_{\rm SCF}$ can turn out to be crucial. We demonstrate this point by showing potential energy distribution (PED) (shown in Fig. 1) calculated using two different $\Delta E_{\rm SCF}$ criteria, 0.0001 and 0.000 01 a.u., for two temperatures 40 and 175 K. Let us recall that PED(E,T) denotes accessible energy states between E and $E+dE$ (where E is total electronic energy of the system). Figure 1 clearly shows that two different $\Delta E_{\rm SCF}$

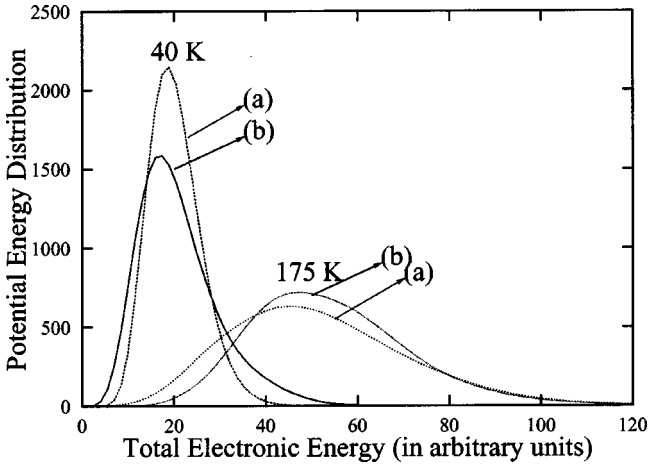

FIG. 1. Comparison of PED for 40 and 175 K using different criteria for convergence in the total electronic energy (ΔE_{SCF}). (a) denotes $\Delta E_{\mathrm{SCF}} = 0.000\,01$ a.u. and (b) denotes $\Delta E_{\mathrm{SCF}} = 0.0001$ a.u.

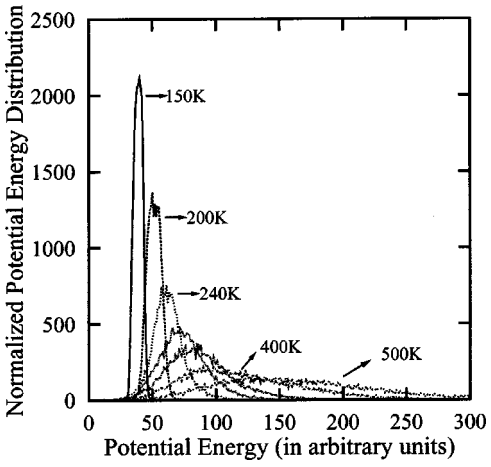

FIG. 3. Normalized potential energy distribution of Li_7 for some relevant temperatures; *viz* 150, 200, 240, 280, 320, 400, and 500 K. It should be noted that PED for 400 and 500 K are very flat and almost overlapping.

leads to considerably different PEDs. The height of the peak in Fig. 1(a) (i.e., $\Delta E_{\mathrm{SCF}} = 0.000\,01$ a.u.) is about 25% higher than Fig. 1(b) (i.e., $\Delta E_{\mathrm{SCF}} = 0.0001$ a.u.) at 40 K. Further, it can be seen that the lower accuracy curve is seen to span a broader energy range and we have verified that this leads to the erroneous specific heat in this range of temperatures. However, as the temperature rises lower criteria can be used without lose of accuracy.

III. RESULTS AND DISCUSSIONS

A. Finite temperature behavior of host cluster: Li_7

We begin our discussion by examining the equilibrium geometries of Li_7 (shown in Fig. 2). The ground-state structure is a pentagonal bipyramid with D_{5h} symmetry. The excited state is tricapped tetragon (C_{2v} symmetry) with 0.22 eV higher in energy compared to the ground state. These geometries are consistent with the earlier reported work.[24] As expected the charge distribution is completely delocalized indicating metallic like bonding in this cluster (not shown).

Before discussing the thermodynamic quantities like specific heat it is instructive to examine normalized potential energy distribution (PED) obtained via our molecular-dynamic simulations, as a function of temperature. In Fig. 3 we show PED for different temperatures ranging from 150 to 500 K. It may be noted from Fig. 3 that the PED for low temperatures is very sharp and narrow indicating that the system spans a very restricted range of energies. Indeed the observed motion at these temperatures shows that atoms oscillate around their equilibrium positions. As temperature increases the pumped in energy is used to break some of the bonds and as a result cluster spans wider configuration space which reflects in the broader PED. We note that around 400 K the PED becomes very flat which indicates that the cluster is spanning large number of energy states with equal probability. This rather broad PED around 400 K and above as

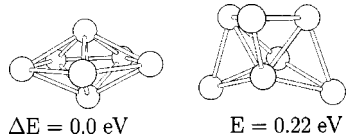

FIG. 2. The ground state and the first excited-state geometry of Li_7. ΔE represents difference in the total energies.

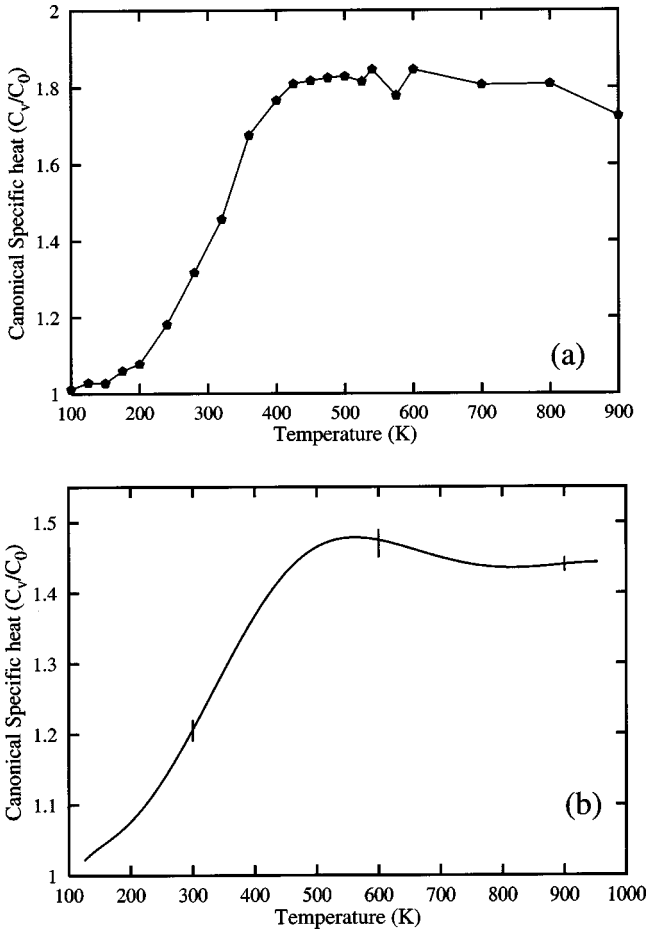

FIG. 4. The canonical ionic specific heat of Li_7. (a): Computed directly from fluctuations using Eq. (1) with 75 ps for temperatures up to 200 K and 150 ps or more for higher temperatures. (b): The specific heat curve calculated using multihisto fit.

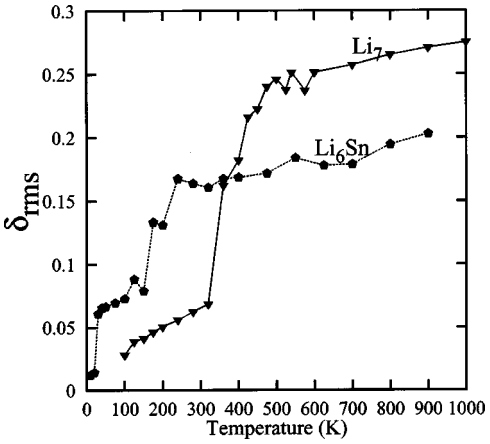

FIG. 5. Root-mean square bond length fluctuations of Li_7 and Li_6Sn. The slow monotonous rise in δ_{rms} for Li_7 below 320 K indicates solidlike behavior whereas linear nature above 450 K shows liquidlike behavior. For Li_6Sn the Lindmann criteria gets satisfied at a much lower temperature (around 175 K). We also note that for Li_6Sn the value of δ_{rms} remains considerably constant for a wide range of temperature, i.e., from 250 to 700 K.

compared to the PED for lower temperatures is suggestive of liquidlike nature of the cluster in this range of temperatures.

Some insight can be gained by observing the detailed motion (the movie) of the cluster at few interesting temperature. We note that, around 360 K cluster starts revisiting the ground state via the first excited state and during this process, atoms from the pentagonal ring and atoms capping the ring get interchanged. This processes of interchanging of atoms, becomes more frequent with increasing temperature. Indeed as we shall see this behavior leads to the peak in the specific heat around 425 K. In Fig. 4 we show ionic specific heat of Li_7 calculated using Eq. (1) directly [shown in Fig. 4(a)] as well as with the multiple histogram technique [shown in Fig. 4(b)]. Evidently, both the methods yield similar specific heat except that specific heat by MH is much smoother. We note that the specific heat is very broad and does not change significantly after the peak around 425 K. Such a broad peak in the specific heat is a characteristic of small clusters in contrast to the sharp transition observed in the extended systems.

These observations are also supported by the δ_{rms} which is shown in Fig. 5. As the name suggest δ_{rms} indicates fluctuations in the bond lengths averaged over all pairs and simulation time. According to the Lindmann criteria the clusters are considered to be in the liquidlike state when δ_{rms} exceeds 0.1. It is interesting to note that δ_{rms} shows three distinct regions, a solidlike region below 320 K and a liquidlike region above 450 K. 320–450 K is a transition region and the value of δ_{rms} rises sharply in this region. If we chose to use the Lindmann criteria to estimate the ''melting temperature'' then this cluster ''melts'' between 320 and 360 K.

In Fig. 6 we show the power spectra of Li_7 for six different temperatures. Let us recall that oscillatory motions give rise to one or more discrete peaks in the power spectra whereas the diffusive motion is signaled by the nonzero amplitude at $\omega=0$. As expected, for low temperatures (up to 250 K) we observe a single peak, indicating purely oscillatory

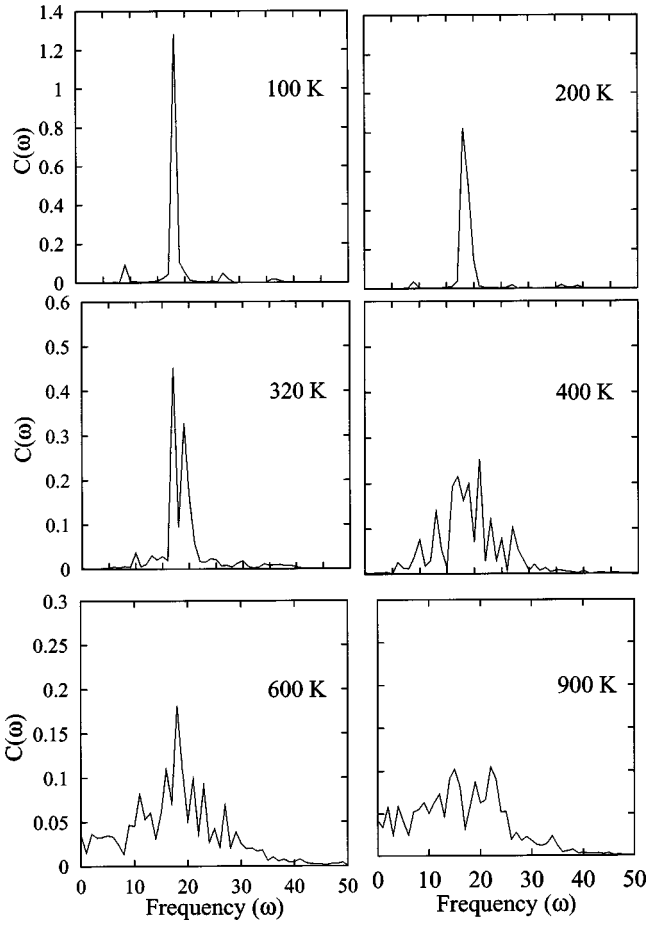

FIG. 6. The power spectra of Li_7 for six different temperatures.

motion up to that temperature. As temperature increases, more frequencies appear in the power spectra, which implies that the motion at that temperature is a combination of all these modes of oscillations. Still the nature of the spectrum is discrete and the cluster is in solidlike state. Around 500 K we begin to see the nonzero value of $\omega=0$ frequency in the power spectra which is a signature of diffusive motion and hence liquidlike state. We also note that, with increasing temperature, the discrete nature of power spectra changes to continuous one.

To summarize, the specific heat curve indicates that above 425 K Li_7 is definitely *liquidlike* and the transition is characterized by rather broad peak in the specific heat. These features are consistent with the specific heat of Li_8 reported in Ref. 25. Both these clusters namely Li_7 and Li_8 do not show any premelting features.

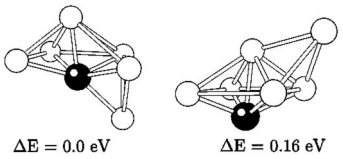

FIG. 7. The ground-state and the first excited-state geometry of Li_6Sn. ΔE represents difference in the total energies.

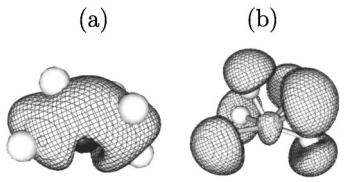

FIG. 8. The isosurfaces for difference charge-density of Li_6Sn. (a): Charge gained region, (b): Charge depletion region. Sn is shown by the black sphere at the center whereas white spheres indicate Li atoms.

B. Finite temperature behavior of impurity doped cluster: Li_6Sn

In this section we present our results on the impurity doped cluster, namely Li_6Sn and contrast the behavior with that of host cluster Li_7.

Before studying these finite temperature effects let us examine the equilibrium structures of Li_6Sn which are shown in Fig. 7. First, we note that both the geometries are considerably different than that of Li_7. Second, in the ground state, Sn has sixfold coordination whereas the first excited state which is 0.16 eV above the ground state, has fivefold coordination with Li atoms. Thus the first excited state has one less Li–Sn bond. Further, these two structures can be obtained by capping the most stable Li_4Sn tetrahedron[14] in two different ways.

Now we turn to the bonding features of the system. Our earlier work[14] has shown that a tetravalent impurity like Sn in lithium clusters changes the delocalized metalliclike bonding to dominantly ionic like. For the sake of completeness we discuss the bonding characteristics in brief. Toward this end, in Fig. 8 we show the difference charge density of Li_6Sn, defined as the difference between the selfconsistent charge density and the superimposed atomic charge density. Quite clearly, the charge gained region is mainly around Sn whereas the charge depletion region is near all Li atoms. This clearly shows that there is a charge transfer from all Li atoms to Sn, filling in the Sn centered *p* orbitals.[26] Typically the depleted charge is of the order of 2/3 electron per Li atom. As a consequence of the significant charge transfer from Li to Sn, considerable depletion of charge in the region of Li–Li bond is observed which results into weakening of Li–Li bond. This weakening of Li–Li bonds show dramatic effects on the finite temperature behavior of the cluster.

The consequences of weakening of Li–Li bonds are observed at very low temperatures. Around 30 K two Li–Li bonds break and Li atoms get separated into two bunches (see Figs. 9(b) and 9(c)]. These bunches perform a constrained motion around Sn as shown in Fig. 9. We note from Fig. 9 that the initial [Fig. 9(a)] and final [Fig. 9(d)] geometries are same but have different orientations. Since the motion is observed at very low temperatures the potential barrier joining these two (identical) structures must be very low. The effect of this motion shows up in the PED of Li_6Sn. In Fig. 10 we compare PED of Li_6Sn with that of Li_7. Evidently, at 150 K the PED of Li_6Sn is significantly different than that of Li_7. A rather narrow and sharp distribution for Li_7 indicates that it is showing clear solidlike behavior exhibiting small oscillations at this temperature, whereas the significantly broader distribution of Li_6Sn indicates that other modes of excitations are also available to the system around this temperature. In fact the observed motion at this temperature shows breaking of most of the Li–Li bonds. On the other hand at 400 K the PED of both clusters have similar shapes.

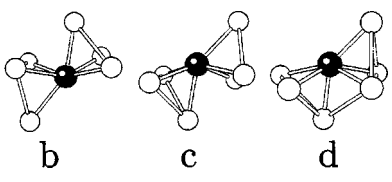

FIG. 9. Actual snap shots of a typical low temperature motion of Li atoms around Sn depicting passage of the cluster between two identical structures (a) and (d); (a): The ground state geometry [(b) and (c)]: Two Li–Li bonds are broken and the Li atoms get separated into two bunches which form a constrained motion around Sn. (d): The resultant geometry.

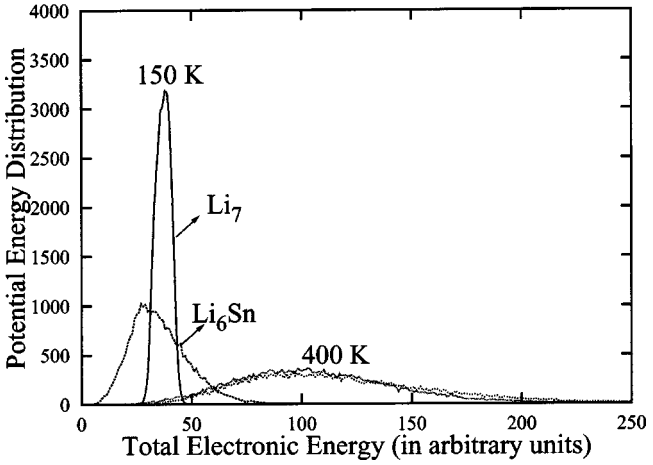

FIG. 10. Normalized potential energy distribution at 150 and 400 K of Li_6Sn and Li_7.

Turning to the ionic specific heat of Li_6Sn (shown in Fig. 11) we note that the specific heat curve is significantly different than that of Li_7. Unlike Li_7, it shows a shoulder around 50 K (Ref. 27) and the main peak is observed at substantially lower temperature (i.e., 250 K) compared to that of Li_7 (425 K). The shoulder in the specific heat curve of Li_6Sn corresponds to the low temperature motion described

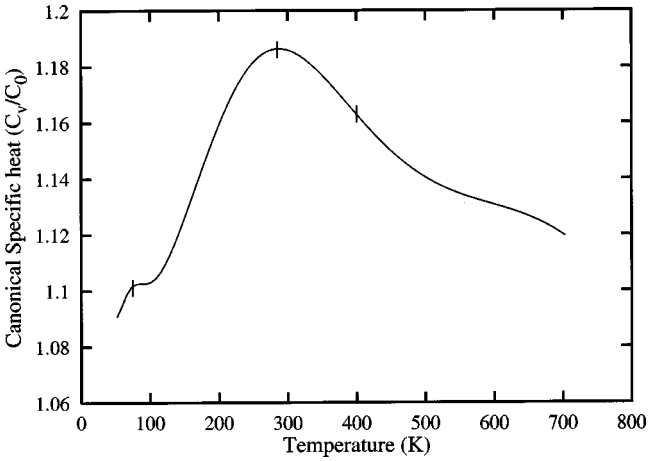

FIG. 11. The canonical ionic specific heat of Li_6Sn. The peak is around at 250 K which is substantially lower than observed in Li_7.

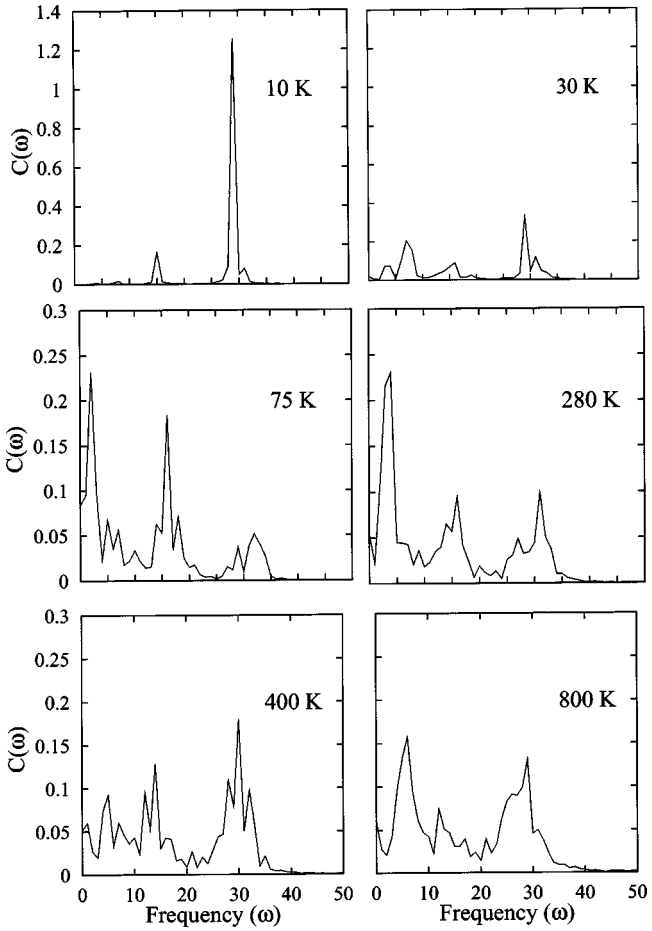

FIG. 12. The power spectra of Li_6Sn for six different temperatures.

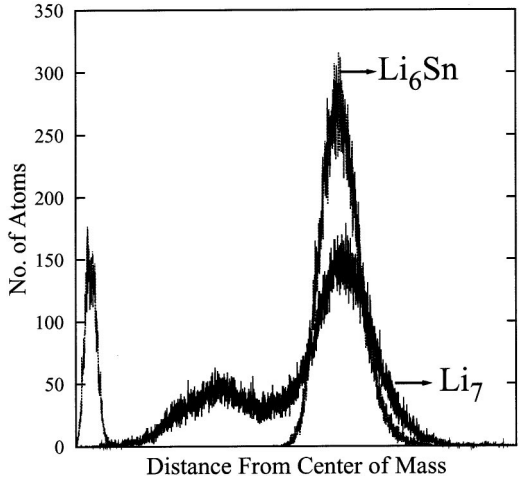

FIG. 13. The distribution of atoms from center of mass at 700 K in Li_6Sn and Li_7. The *y* axis is not normalized.

earlier. As temperature rises further this constrained motion becomes more rigorous and eventually around 200 K the bunches of Li atoms lose their identity and exhibit diffusive motion around Sn. This leads to the peak around 250 K in the specific heat.

In Fig. 12 we show the power spectra of Li_6Sn. It may be noted that the power spectra of Li_6Sn is significantly different than that of Li_7. In case of Li_7 up to 250 K we observe a single prominent peak whereas in Li_6Sn, we note that at very low temperatures (around 30 K) a range of frequencies contribute to the motion of the cluster. The amplitude of the prominent peak seen at 10 K (due to the oscillatory motion) has considerably reduced with appearance of some low frequencies in the spectra. These low frequencies are identified with the motion motion of Li atoms seen at that temperature. Around 75 K we observe a nonzero value of the DC component of power spectra. We also note that the power spectra for 400 and 800 K are similar in nature indicating that the cluster is in liquidlike state in this temperature range.

These observations are consistent with the δ_{rms} which is shown in Fig. 5 along with the δ_{rms} for Li_7. For Li_6Sn the value of δ_{rms} rises in two distinct steps. The first step is around 30 K. We recall that it is at this temperature the diffusive motion of Li atoms (in bunches) begins and another step is around 200 K where the bunches of Li atoms lose their identity and diffuse around Sn.

It is interesting to note that, though the value of δ_{rms} does not show an appreciable rise from 250 to 700 K, indicating that the cluster is in liquidlike state, the kind of motion observed in this temperature range, in Li_6Sn is quite different than that of Li_7. To illustrate this point, in Fig. 13 we show the distribution of atoms as a function of distance from center of mass. It may be noted that even at as high temperature as 700 K, Li atoms in Li_6Sn are mostly in a shell of thickness 2 a.u. and at a distance of 5 a.u. around Sn (Sn being heavy, it is very close to the center of mass and the peak near the origin is because of the Sn atoms). It is obvious from Fig. 13 that the motion of Li atoms in Li_7 is quite similar to the one expected in homogeneous liquids.

Thus our calculations indicate that the main peak in specific heat of Li_6Sn, around 250 K is associated with the breaking of weak Li–Li bonds while retaining the bonding between Li and Sn. We also note that in Li_6Sn, though δ_{rms} satisfies the Lindmann criteria at very low temperature compared to that of Li_7, its saturated value is 0.17 which is considerably lower compared to the host Li_7 ($\delta_{\mathrm{rms}}=0.25$) cluster. This indicates that in the liquid-state the volume expansion of the impurity system is much less than in the case of the host cluster.[28] This is consistent with the existence of stronger Li–Sn bond in the system. At still higher temperatures one of the ionic bonds breaks and we observe the first excited state (shown in Fig. 7) in which Sn has one less coordination number than the ground state. Thus the route for evaporation proceeds via the first excited state. Finally we note that, Li_6Sn is an over lithiated cluster, i.e., the number of Li atoms in the cluster are more than those required to complete the *p* shell of Sn atom. It will be interesting to investigate the finite temperature behavior of a cluster which satisfy the octet rule, i.e., like $Li_{4x}Sn_x$. In these clusters though we expect that because of *complete* charge transfer from all Li atoms to Sn, the bonds between Li atoms will be extremely weak, the ionic bond between Li–Sn will be more strong than those in the over-lithiated cluster like Li_6Sn.

IV. CONCLUSIONS

We have presented an *ab initio* isokinetic MD simulations on Li_6Sn and Li_7 to demonstrate the dramatic effects

induced by the impurity in the host cluster. The key point which emerges out of these calculations is that the essential physics governing these effects comes from the charge transfer from Li to Sn because of the large difference in their electronegativities. In Li_6Sn, we observe a beginning of diffussive motion of Li atoms (around Sn) at very low temperature which gives rise to a shoulder in the specific heat curve around 50 K. The main peak is observed at much lower temperature, around 250 K, compared to the host cluster ($\approx$425 K) whereas Li_7 shows a broad peak in the specific heat with no premelting features. The motion in the liquid state of Li_6Sn is essentially a constrained motion of Li atoms around Sn center.

ACKNOWLEDGMENT

We gratefully acknowledge the financial support of the ISRO-DRDO, India.

[1] *Physics and Chemistry of Finite Systems: From Clusters to Crystals*, edited by P. Jena, S. N. Khanna, and B. K. Rao (Kluwer Academic, Dordrecht, Netherlands, 1992), Vols. 1 and 2.
[2] *Clusters and nanostructured Materials*, edited by P. Jena and S. N. Behera (Nova Science Publishers, Inc., New York, 1996); Vijay Kumar, E. Esfarjini, and Y. Kawazoe, *Advances in Cluster Science* (Springer-Verlag, Heidelberg, 2000).
[3] W. A. de Heer, Rev. Mod. Phys. **65**, 611 (1993).
[4] Matthias Brack, Rev. Mod. Phys. **65**, 677 (1993).
[5] T. P. Martin, Phys. Rep. **273**, 199 (1996).
[6] B. K. Rao and P. Jena, J. Chem. Phys. **113**, 1508 (2000); J. A. Alonso, L. M. Molina, M. J. Lopez, A. Rubio, and M. J. Stott, Chem. Phys. Lett. **289**, 451 (1998); H.-P. Cheng, R. N. Barnett, and U. Landman, Phys. Rev. B **48**, 1820 (1993).
[7] M. Deshpande, A. Dhavale, R. R. Zope, S. Chacko, and D. G. Kanhere, Phys. Rev. A **62**, 063202 (2000); R. R. Zope, S. A. Blundell, T. Baruah, and D. G. Kanhere, J. Chem. Phys. **115**, 2109 (2001); S. Chacko, M. Deshpande, and D. G. Kanhere, Phys. Rev. B **64**, 155409 (2001); M. Deshpande, D. G. Kanhere, P. V. Panat, I. Vasiliev, and R. M. Martin, Phys. Rev. A **65**, 053204 (2002); A. Dhavale, D. G. Kanhere, S. A. Blundell, and R. R. Zope, Phys. Rev. B **65**, 085402 (2002), and references therein.
[8] M. Schmidt, R. Kusche, W. Kronmüller, B. von Issendorff, and H. Haberland, Phys. Rev. Lett. **79**, 99 (1997); Nature (London) **393**, 238 (1998).
[9] A. A. Shvartsburg and M. F. Jarrold, Phys. Rev. Lett. **85**, 2530 (2000).
[10] A. Vichare, D. G. Kanhere, and S. A. Blundell, Phys. Rev. B **64**, 045408 (2001); P. Blaise and S. A. Blundell, *ibid.* **63**, 235409 (2001); A. Rytkönen, H. Häkkinen, and M. Manninen, Phys. Rev. Lett. **80**, 3940 (1998); A. Aguado, J. M. Lopez, J. A. Alonso, and M. J. Stott, J. Chem. Phys. **111**, 6026 (1999).
[11] K. Joshi, D. G. Kanhere, and S. A. Blundell, Phys. Rev. B **66**, 155329 (2002).
[12] K. Joshi, D. G. Kanhere, and S. A. Blundell, Phys. Rev. B **67**, 235413 (2003).
[13] D. G. Kanhere, A. Vichare, and S. A. Blundell, *Reviews in Modern Quantum Chemistry*, edited by K. D. Sen (World Scientific, Singapore, 2001); T. L. Hill, *The Thermodynamics of Small Systems Part I* (Benjamin, New York, 1963); *The Thermodynamics of Small Systems Part II* (Benjamin, New York, 1963).
[14] K. Joshi and D. G. Kanhere, Phys. Rev. A **65**, 043203 (2002).
[15] W. van der Lugt, J. Phys.: Condens. Matter **8**, 6115 (1996); O. Genser and J. Hafner, *ibid.* **13**, 959 (2000); **13**, 981 (2000); Phys. Rev. B **63**, 144204 (2001).
[16] P. H. K. de Jong, P. Verkerk, W. van der Lugt, and L. A. de Graaf, J. Non-Cryst. Solids **156–158**, 978 (1993).
[17] D. L. Price, M.-L. Saboungi, and W. S. Howells, Phys. Rev. B **51**, 14923 (1995).
[18] M. C. Payne, M. P. Teter, D. C. Allen, T. A. Arias, and J. D. Joannopoulos, Rev. Mod. Phys. **64**, 1045 (1992).
[19] G. B. Bachelet, D. R. Hamman, and M. Schlüter, Phys. Rev. B **26**, 4199 (1982).
[20] L. Kleinman and D. M. Bylander, Phys. Rev. Lett. **48**, 1425 (1982).
[21] D. M. Ceperley and B. J. Alder, Phys. Rev. Lett. **45**, 566 (1980).
[22] D. J. Evans and G. P. Morriss, *Statistical Mechanics of Non-Equilibrium Liquids* (Academic, London, 1990).
[23] A. M. Ferrenberg and R. H. Swendsen, Phys. Rev. Lett. **61**, 2635 (1988); P. Labastie and R. L. Whetten, *ibid.* **65**, 1567 (1990).
[24] I. Boustani, W. Pewestorf, P. Fantucci, V. Bonačić-Koutecký, and J. Koutecký, Phys. Rev. B **35**, 9437 (1987); R. O. Jones, A. I. Lichtenstein, and J. Hutter, J. Chem. Phys. **106**, 4566 (1997).
[25] S. Srinivas and J. Jellinek, Phys. Status Solidi B **217**, 311 (2000).
[26] We have examined the relevant occupied orbitals and have observed that all the orbitals are centered around Sn.
[27] We have verified the existence of this small shoulder by carrying out a number of additional simulations between 10 and 100 K.
[28] This is also confirmed by calculating the distance of the farthest atom from center of mass of the cluster averaged over 60 ps. For Li_7 this distance is 4.78 a.u. at 100 K and 5.15 a.u. at 900 K (increased by 0.37 a.u.) whereas for Li_6Sn it is 4.75 a.u. at 125 K which has raised to 4.84 a.u. at 900 K (increased by 0.09 a.u.).